J Nanopart Res (2020) 22: 191
https://doi.org/10.1007/s11051-020-04933-4

RESEARCH PAPER

CO_2 adsorption performance of CuBTC/graphene aerogel composites

Wen Ren · Zhenzhen Wei · Xiaoxiao Xia · Zhiwei Hong · Song Li

Received: 6 March 2020 / Accepted: 25 June 2020 / Published online: 2 July 2020
© Springer Nature B.V. 2020

Abstract Metal-organic frameworks (MOFs) have been recognized as promising adsorbents for carbon capture due to their ultrahigh surface areas and tunable properties. However, a majority of MOFs have strict requirements for preparation and high mass transfer resistance that limits the gas separation time. In order to improve the applicability of MOFs to practical applications, herein, we reported an experimental approach to prepare structured CuBTC/graphene aerogel (GA) composites using ionic liquid (IL) additives (CuBTC/GA-IL) at room temperature for CO_2 capture. The material was characterized by powder X-ray diffraction (PXRD), scanning electron microscopy (SEM), specific surface area analysis, and CO_2 adsorption tests. It was demonstrated that CuBTC/GA-IL exhibited the higher CO_2 uptake than CuBTC/GA prepared without IL additives. Besides, the breakthrough experiments have shown that CuBTC/GA-IL exhibited the lower mass transfer resistance compared with CuBTC-IL and good cyclability. The effective approach of fabricating CuBTC into GA using IL additives to improve CO_2 adsorption in this study may be extensively applied for other MOF-based composites.

Keywords Metal-organic frameworks · Graphene aerogel · Composite · Carbon capture · Ionic liquids · Nanomaterials

Wen Ren and Zhenzhen Wei are co-authors.

Electronic supplementary material The online version of this article (https://doi.org/10.1007/s11051-020-04933-4) contains supplementary material, which is available to authorized users.

W. Ren · Z. Wei · X. Xia · Z. Hong · S. Li
State Key Laboratory of Coal Combustion, School of Energy and Power Engineering, Huazhong University of Science and Technology, Wuhan 430074 Hubei, China

W. Ren · S. Li (✉)
China-EU Institute for Clean and Renewable Energy, Huazhong University of Science and Technology, Wuhan 430074 Hubei, China
e-mail: songli@hust.edu.cn

Introduction

Massive reduction of CO_2 content in the atmosphere is of great importance to alleviate greenhouse effects for sustainable development (Boothandford et al. 2014; Gibbins et al. 2008). Among CO_2 capture technologies, physical adsorption by microporous materials is a promising option because of its cost-effectiveness and high efficiency (Yu et al. 2017). Various porous materials have been used for carbon capture, such as activated carbon, zeolites, and metal-organic frameworks (MOFs) (Trickett et al. 2017; Xiang et al. 2012). In recent years, MOFs have been increasingly investigated for gas adsorption and separation (Li et al. 2018b; Li et al. 2011; Wang et al. 2018) due to their ultrahigh surface areas, pore volumes, and structure tunability. Among all the reported MOFs, CuBTC (also known as HKUST-1 or MOF-199) (Chui et al. 1999) has been widely studied and commercialized because

of its excellent textural properties and outstanding CO_2 adsorption performance.

However, the limitations that restrict the widespread application of CuBTC for carbon capture still exist. One of the limitations for CuBTC is the strict synthesis conditions including high temperature and pressure required. Therefore, seeking a mild synthesis condition is attractive to promote the industrialization of CuBTC. Recently, Na et al. (2015) reported a strategy to successfully prepare CuBTC with a rapid and energy-efficient approach at room temperature by converting the ligand trimesic acid (H_3BTC) to K_3BTC prior to reaction with metal node. However, the structure property of obtained CuBTC including specific surface area and crystallinity is not as high as that by conventional hydrothermal synthesis. Previous studies also reported that ionic liquids (ILs) could assist ionothermal synthesis of MOFs. Liu et al. (2010) successfully synthesized two new MOFs by changing the solvent from water to ILs. Besides, the crystalline morphology of MOFs can be modified by tuning the cation/anion types of ILs (Shang et al. 2013). The addition of [Bmim][PF_6] is favorable for Zn-MOF preparation at room temperature (Ye et al. 2018). Bian et al. (2014) reported triethylene tetramine acetate (TETA-Ac) was able to assist the growth of CuBTC on graphene oxide sheets, thus leading to improve CO_2 uptake of 5.62 mmol/g at 25 °C and 1 bar. Such findings may be ascribed to the additional active sites provided by solvation environment of ILs for the adsorption of Cu^{2+} cations through the coordination, which can benefit the initial growth of the CuBTC, thus leading to the improvement in the structure property and adsorption performance.

Hierarchical pores of adsorbents providing the lower mass transfer resistance are favorable for rapid adsorption/desorption cycles (Rezaei and Webley 2010). However, a vast majority of MOFs reported to date possess micropores and high mass transfer resistance that are unfavorable for fast cycling (Ge et al. 2013; Rezaei et al. 2010). Many efforts have been devoted to explore MOFs with hierarchical pores by using the longer organic spacers or surfactants (Qiu et al. 2008; Wang et al. 2006; Zhao et al. 2011). However, such an approach is complicated and difficult to manipulate. Thus, MOF-based composites were fabricated by integrating MOFs into mesoporous alumina (Gorka et al. 2010), mesoporous silica (Chen et al. 2018), MCM-41 (Furtado et al. 2011), mesoporous carbon nanotubes (CNTs) (Xiang et al. 2011), and multiwall CNTs (Anbia and Hoseini 2012), most of which displayed hierarchical pores and improved adsorption performance. Very recently, graphene aerogel (GA) with meso-/macropores has been used as an alternative support for growing MOFs. MOF/GA composites by incorporating MOFs into the aerogel matrix have been winning increasing attentions due to their synergistic effect on adsorption performance (Inonu et al. 2018). In recent years, MIL-101(Cr)/GA for drug extraction (Zhang et al. 2016), ZIF-8/rGO aerogel for water remediation (Mao et al. 2017), and Zr-MOF (MMU)/GA for solid phase extraction (Li et al. 2018a) have been exploited. The CO_2 adsorption performance of ZIF-8/GA was recently reported, in which a hierarchical hybrid ZIF-8/GA exhibited a CO_2 uptake of 0.99 mmol/g and mechanical robustness (Jiang et al. 2018). In order to improve the CO_2 adsorption capacity, reduce the mass transfer resistance, and achieve the mild synthesis of CuBTC, in this work, we prepared a hybrid CuBTC/GA composite with ILs as additives at room temperature for CO_2 adsorption. The structure characterization, CO_2 adsorption, and breakthrough measurement demonstrated that CuBTC/GA composites are promising adsorbents for carbon capture.

Experimental

Chemicals

All chemicals were used as received (without any purification) from commercial sources. Graphite powder (325 mesh) and benzene-1,3,5-tricarboxylic acid (H_3BTC, 98%) were purchased from Shanghai Aladdin Bio-Chem Technology Co. Potassium permanganate ($KMnO_4$, AR), L-ascorbic acid (AR), hydrogen peroxide (H_2O_2, 30%), copper nitrate trihydrate ($Cu(NO_3)_2{\cdot}3H_2O$, AR), sodium hydroxide (NaOH, AR), 1-butyl-3-methyllmldazollum tetrafluoroborate ([Bmim][BF_4], 97%), ethanol (AR), and concentrated sulfuric acid (H_2SO_4, 98%) were purchased from Shanghai Sinopharm Chemical Reagent Co. Deionized water (DI) was produced using the pure water filter (SMART-N) in our laboratory. Carbon dioxide (CO_2, 99.99%), nitrogen (N_2, 99.99%), and helium (He, 99.999%) gases were purchased from Wuhan Huaerwen Co.

Materials preparation

Graphene aerogel Prior to GA preparation, graphene oxide (GO) was prepared from the natural graphite

powder (325 mesh) according to a modified Hummers method (Jiang et al. 2018). Firstly, graphite powder (2 g), $KMnO_4$ (6 g), and concentrated H_2SO_4 solution (120 mL) were stored in a refrigerator (− 18 °C) for 30 min and graphite was added to cold concentrated H_2SO_4 with stirring for 2 h in an ice bath. Secondly, the mixture was stirred at 50 °C for 6 h in an oil bath and diluted with deionized (DI) water (240 mL). After adding DI water, H_2O_2 solution was slowly added into the mixture until no bubble appeared. Finally, the product was washed repeatedly with deionized water by centrifugation until the filtrate became almost neutral. The resulting brown-yellow product is GO. GA was obtained by reducing GO with L-ascorbic acid (Jiang et al. 2018). Firstly, 80 mg L-ascorbic acid was added to 10 mL GO aqueous dispersion (4 mg/L), and the mixture was stirred at 95 °C for 25 min to form a partially reduced graphene hydrogel (GH). Then, the GH was totally frozen in a refrigerator (− 18 °C) followed by thawing at room temperature and were terminated in the reduction period for another 10 min. After the reaction, the GH was solvent exchanged with ethanol for three times. Finally, GA was obtained by drying GH at 60 °C for 12 h.

CuBTC-IL First of all, different molar ratios of Cu^{2+} and [Bmim][BF_4] (1:2, 1:1, 2:1, 3:1, and 4:1) were tested to optimize the amount of added ILs. The PXRD patterns and Brunauer-Emmett-Teller (BET) surface areas shown in Fig. S1 and Fig. S2 demonstrated that the molar ratio of 2:1 gave rise to the highest BET surface areas without compensating the crystallinity. Therefore, 2:1 was chosen for CuBTC-IL preparation. Then, the Cu^{2+}-[Bmim][BF_4] solution (0.2 mol/L) was obtained by dissolving $Cu(NO_3)_2{\cdot}3H_2O$ (0.435 g, 1.8 mmol) in the deionized water (9 mL) followed by adding [Bmim][BF_4] (0.203 g, 0.9 mmol). Na_3BTC solution (0.1 mol/L) was obtained by dissolving H_3BTC (0.252 g, 1.2 mmol) and NaOH (0.144 g, 3.6 mmol) in the deionized water (12 mL). Finally, Na_3BTC solution was added into the Cu^{2+}-[Bmim][BF_4] solution slowly under stirring for 2 min, followed by solvent exchange with ethanol for three times (3 × 30 mL). The final products were dried in an oven at 80 °C for 24 h to obtain CuBTC-IL. For CuBTC preparation, the same procedure was employed without [Bmim][BF_4].

CuBTC/GA-IL GA was soaked in Cu^{2+}-[Bmim][BF_4] solution (9 mL, 0.2 mol/L) for 2 h at room temperature, followed by adding Na_3BTC solution (12 mL, 0.1 mol/L) under mild stirring for 2 min. The obtained solution was kept standing still for 30 min, followed by solvent exchange with ethanol for three times (3 × 30 mL). The obtained product was collected by suction filtration. Finally, the products were dried in an oven at 80 °C for 24 h. The process was depicted in Scheme 1. For CuBTC/GA preparation, the only difference is the use of Cu^{2+} solution for GA soaking.

Characterization

Powder X-ray diffraction (PXRD) patterns of all samples were collected on a PANalytical X'Pert X-ray diffractometer equipped with an X'Celerator detector module and using Cu Kα (λ = 1.5418 Å) radiation, with a step size of 0.013° in 2θ. All data were collected at an ambient temperature with the measurement angle ranging from 5° to 50°. Scanning electron microscopy (SEM) images were obtained using a field emission SEM (S4800) at an accelerating voltage of 5 kV. Surface areas and pore volumes were obtained from nitrogen adsorption isotherms measured at 77 K on the Autosorb-iQ2 sorption analyzer of Quantachrome Instruments. Brunauer-Emmett-Teller (BET) surface areas were determined by fitting the BET model to the collected isotherms.

Gas adsorption tests

N_2 and CO_2 adsorption isotherms of all samples were measured on Quantachrome Autosorb-iQ2 sorption analyzer at 298 K. Prior to measurement, all samples were outgassed at 423 K for 24 h under dynamic vacuum. N_2 and CO_2 adsorption isotherms were measured from 0 to 1 bar. The temperature was controlled by immersing sample cells in circulating water bath. Breakthrough experiment was performed in a fixed adsorption bed (VDSORB-200) (40 cm in length and 6 mm in diameter) to investigate the dynamic adsorption performance of adsorbents. CuBTC-IL, GA, and CuBTC/GA-IL samples were loaded into the center of cylindrical adsorption column without additional compression. Each sample filled 5-cm-length adsorption column. A CO_2/N_2 gas mixture (20/80% *v*/*v*) was employed as the influent stream with the total flow rate of 35 mL/min until the concentration of exhaust gas monitored by a mass spectrometer (Cirrus2) does not change. To gain desired gas concentration, CO_2 was first pre-mixed with N_2 in a gas mixer before passing through the adsorption column by adjusting the flow rate. N_2 and CO_2 with high purity were

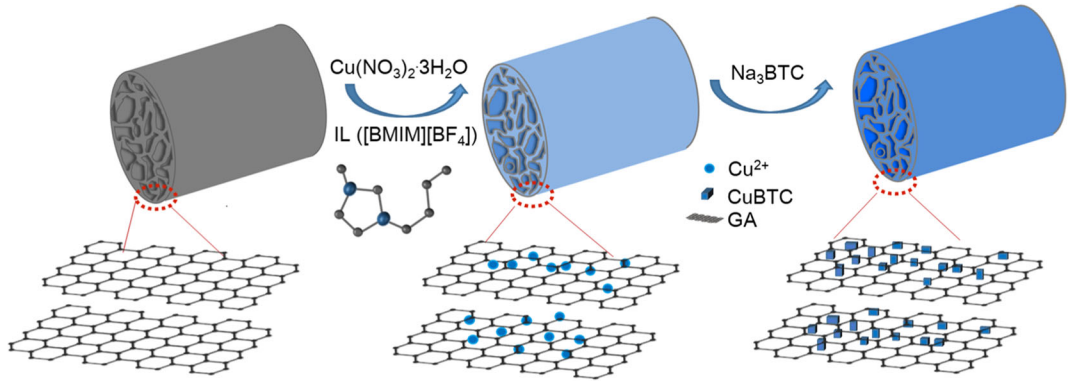

Scheme 1 Schematic synthesis process of CuBTC/GA-IL using ionic liquids (ILs) additives at room temperature.

used and the gas flow rate was adjusted with the flowmeters. The variation in gas concentration from inlet to outlet during the adsorption process was monitored by mass spectrometer (Cirrus2). All samples were heated at 423 K for 12 h to removal of moisture before loading. After loading, the samples were purged with helium 423 K at a flow rate of 200 mL/min for 2 h to remove the entrapped gas. Then, the temperature was adjusted to 298 K for measurement. After breakthrough measurement, the desorption was carried out by helium purging with a flow rate of 200 mL/min at 423 K for 2 h. The recycle stability of adsorbents was tested by four continuous adsorption/desorption cycles. The CO_2 adsorption capacity of adsorbents was calculated by the following equation.

$$q = \frac{F_0 C_0}{W} \int_0^{\infty} \left(1 - \frac{C}{C_0}\right)$$

where q is the quantity of CO_2 adsorbed per unit mass of adsorbents; C_0 and C are the initial feed and effluent concentrations, respectively; F_0 is the initial total flow rate; and W is the mass of adsorbent.

Result and discussion

According to Scheme 1, CuBTC was successfully incorporated into GA under the assistance of IL additives at room temperature to give rise to structured CuBTC/GA-IL. Comparison of PXRD patterns of CuBTC, CuBTC-IL, CuBTC/GA, and CuBTC/GA-IL (Fig. 1) demonstrated that (1) CuBTC synthesized at room temperature exhibited good crystallinity compared with simulated result; (2) CuBTC was successfully grown in GA regardless of the presence of IL additives; and (3) IL addition did not destroy the crystal structures of CuBTC. It was also noticed that the crystallinity of CuBTC/GA and CuBTC/GA-IL was decreased compared with CuBTC, which may be ascribed to the limited space for crystal growth by integrated GA. SEM image of GA in Fig. 2b shows that GA has a cellular network structure, which is well consistent with the SEM image reported previously (Riaz et al. 2017), and the apparent rod-like assembly of CuBTC can be observed (Fig. 2c), in agreement with previous report (Na et al. 2015). SEM image (Fig. 2d) has clearly shown that the presence of CuBTC crystals in GA and CuBTC were well dispersed on the surface of GA, suggesting that GA can provide a microenvironment for the nucleation of CuBTC. The morphology of CuBTC was altered

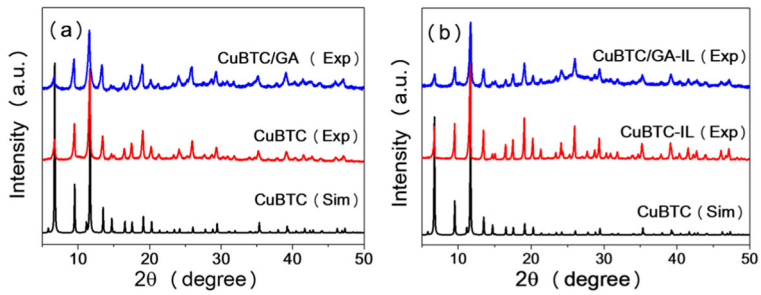

Fig. 1 PXRD patterns of **a** CuBTC and CuBTC/GA; **b** CuBTC-IL and CuBTC/GA-IL

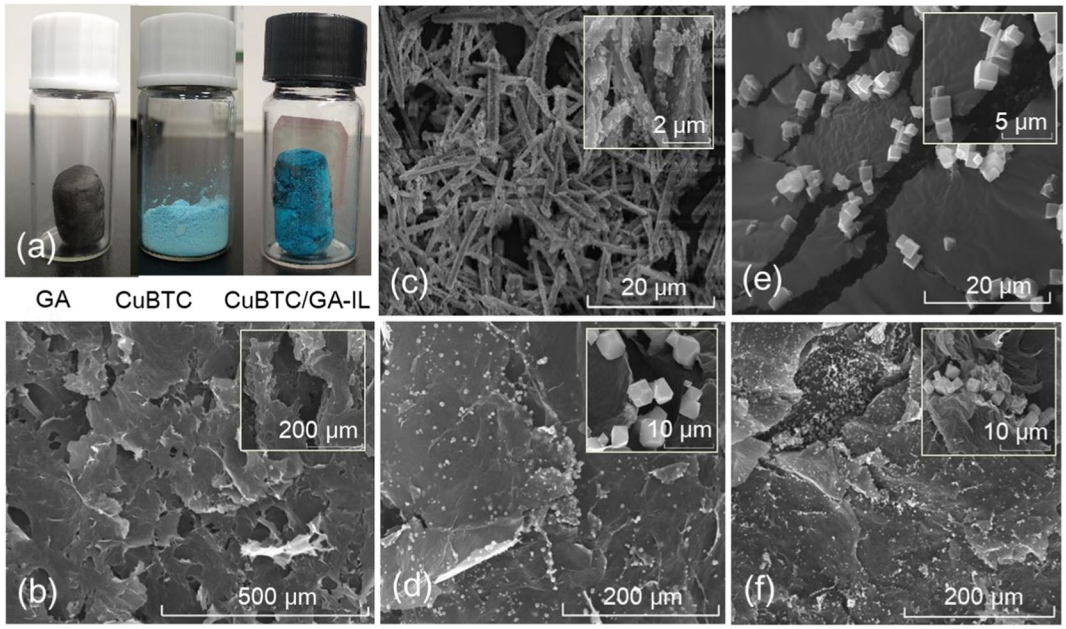

Fig. 2 Photographs of **a** GA, CuBTC, CuBTC/GA-IL, and SEM images of **b** GA, **c** CuBTC, **d** CuBTC/GA, **e** CuBTC-IL, **f** CuBTC/GA-IL

significantly in the presence of ILs (Fig. 2e), in which the cube-shaped CuBTC-IL was observed, which can be assigned to the presence of ILs that can act as nucleation sites for CuBTC growth via heterogeneous nucleation (Bian et al. 2014). SEM image (Fig. 2f) has shown the CuBTC crystals were uniformly distributed on the surface of GA (same as Fig. 2d) with the addition of ILs.

BET surface areas and pore volumes of the samples (Table 1) illustrated that IL addition could remarkably enhance the surface areas and pore volumes of CuBTC (1120 m^2/g vs. 1701 m^2/g and 0.716 cm^3/g vs. 0.862 cm^3/g), implicating the improved CO_2 uptake of CuBTC-IL. However, upon incorporation of CuBTC into GA, the surface area was obviously reduced (CuBTC/GA: 1048 m^2/g vs. 1120 m^2/g of CuBTC; CuBTC/GA-IL: 1281 m^2/g vs. 1701 m^2/g of CuBTC-IL), similar to the result of ZIF-8/GA (Jiang et al. 2018). However, the pore volume of CuBTC/GA-IL was enhanced compared with CuBTC/GA (0.786 cm^3/g vs. 0.724 cm^3/g of CuBTC/GA), consistent with their trend on CO_2 uptakes. Comparing the surface area of CuBTC/GA-IL with CuBTC/GA (1281 m^2/g vs. 1120 m^2/g) demonstrated that IL additives significantly increased the surface area of CuBTC/GA composite, implicating the superior CO_2 adsorption performance of CuBTC/GA-IL.

Table 1 BET surface area (S_{BET}), pore volume (V_p), and CO_2 uptake (298 K, 1 bar) of GA, CuBTC, CuBTC/GA, CuBTC-IL, and CuBTC/GA-IL

Sample	S_{BET} (m^2/g)	iV_p (cm^3/g)	CO_2 uptake (mmol/g)
GA	464	0.613	0.34
CuBTC	1120	0.716	3.01
CuBTC/GA	1048	0.724	3.26
CuBTC-IL	1701	0.862	4.92
CuBTC/GA-IL	1281	0.786	3.71

The CO_2 adsorption isotherms (Fig. 3) show that GA exhibits the CO_2 uptake of 0.34 mmol/g, consistent with previous report (Jiang et al. 2018), which is significantly lower than CuBTC (3.01 mmol/g). The incorporation of CuBTC into GA slightly enhances its CO_2 uptake (CuBTC/GA, 3.26 mmol/g), which may be ascribed to the high pore volume of composites. On the contrary, the CO_2 uptake of CuBTC/GA-IL is lower than CuBTC-IL due to its low pore volume. Nevertheless, CuBTC/GA-IL still exhibits the higher CO_2 uptake than CuBTC/GA (3.71 mmol/g vs. 3.26 mmol/g), highlighting the importance of IL addition in improving CO_2 adsorption capability. Besides, compared with the CO_2 uptake (4.01 mmol/g) of CuBTC synthesized by conventional hydrothermal method (Liu et al. 2019), CuBTC-IL displayed the increased CO_2 uptake (4.92 mmol/g), especially compared with CuBTC prepared at room temperature (2.77 mmol/g) (Bian et al.

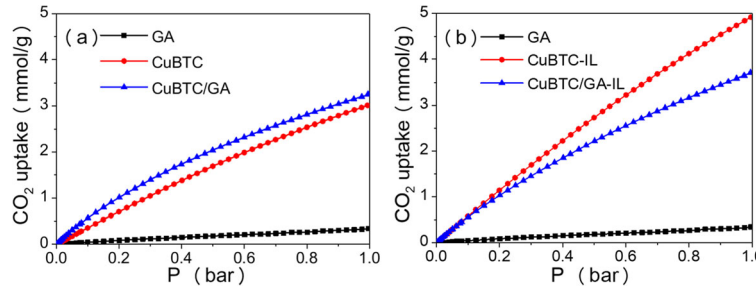

Fig. 3 CO_2 adsorption isotherms of **a** GA, CuBTC, and CuBTC/GA and **b** GA, CuBTC-IL, and CuBTC/GA-IL

2014). In addition, CO_2 uptakes of CuBTC-IL and CuBTC/GA-IL were obviously higher than their N_2 uptakes according to the N_2 and CO_2 adsorption isotherms measured by experiment (Fig. S4), implicating their outstanding CO_2/N_2 selectivity. The CO_2/N_2 selectivities predicted by Ideal Adsorbed Solution Theory (IAST) model (Myers and Prausnitz 1965) based on the CO_2 and N_2 adsorption isotherms of GA, CuBTC-IL, and CuBTC/GA-IL in CO_2/N_2 mixture (20/80% *v*/*v*) of Fig. S3 demonstrated that the CO_2/N_2 selectivity of CuBTC/GA-IL decreased with the pressure (Fig. S5). Moreover, CuBTC/GA-IL exhibited a slightly higher CO_2/N_2 selectivity compared with CuBTC-IL in the low pressure region. However, at 1 bar, CO_2/N_2 selectivity of CuBTC/GA-IL (15.78) was almost identical to that of CuBTC-IL (15.86). Moreover, CuBTC/GA-IL may be more favorable due to the fast mass transfer performance resulting from its hierarchical pores. Thus, both CuBTC/GA-IL and CuBTC-IL were employed for the following breakthrough experiments.

In order to evaluate the dynamic adsorption performance of CuBTC/GA-IL, lab-scale breakthrough experiments were carried out using GA and CuBTC-IL as controls. The obtained breakthrough curve shows C/C_0 (the concentration of a gas of the effluent relative to that of the influent) as a function of time. Breakthrough time of each gas is defined as the time when the C/C_0 achieves 1%. Breakthrough equilibrium time is the time at which the equilibration between effluent and influent concentration was reached. As shown in Fig. 4a, both CO_2 and N_2 were adsorbed before breakthrough; thus, no CO_2 and N_2 were detected. Upon breakthrough, the N_2 concentration was increased firstly at 34 s followed by CO_2 at 144 s, because the CO_2 front propagated slowly due to the high affinity of adsorbents towards CO_2. Therefore, pure N_2 was oversaturated and released, whereas CO_2 was still at adsorbed state during 34–144 s. The discrepancy in the N_2 and CO_2 breakthrough time indicated that CuBTC/GA-IL can separate CO_2 from N_2 during 110 s (Table S1). Eventually, the adsorbent was completely saturated by both CO_2 and N_2, leading to the identical effluent and influent concentration. Comparing the CO_2 breakthrough curves of GA, CuBTC/GA-IL, and CuBTC-IL (Fig. 4b), GA exhibited the shortest breakthrough time (14 s) followed by CuBTC/GA-IL (144 s) and CuBTC-IL (446 s) (Table S1). Besides, the bumps in the breakthrough curve of GA(Fig. 4b) may be contributed by the ultralow mass transfer resistance leading to the fast accumulation of CO_2 molecules inside GA due to its meso-/macropores and low CO_2 uptake (Fig. S7). Moreover, the breakthrough time of CuBTC-IL (446 s) was longer than CuBTC/GA-IL (144 s) (Table S1), implicating the more effective CO_2/N_2 separation (Fig. S8). Besides the short separation time of CuBTC/GA-IL, the calculated CO_2 uptake capacity of CuBTC/GA-IL (2.67 mmol/g) is lower than CuBTC-IL (4.43 mmol/g) according to their breakthrough curves. Such a tendency can be attributed to the low mass transfer resistance due to the hierarchical pores in CuBTC/GA-IL. Thus, small pressure drops and low adsorption capacity can be achieved in CuBTC/GA-IL under rapid cycling (Rezaei and Webley 2010). By tuning the fraction of macro-/mesopores in adsorbents or gas flow rate, the adsorption process of CuBTC/GA-IL may be improved.

Moreover, the front shape of the breakthrough curves is also an important evaluation criteria of mass transfer capability of adsorbents. The mass transfer zone is the region located between breakthrough time and equilibration time (i.e., $C/C_0 = 1$), where the concentration changes most. Besides, reduced mass transfer resistance decreases the adsorption time under rapid cycling. A narrow mass transfer zone is also desired to reduce the energy costs of regeneration (Garcia et al. 2011). In the ideal case, the breakthrough front is a vertical line, implicating that there is no mass transfer resistance and no axial dispersion (García et al. 2011). According to Fig. 4b, the mass transfer zone of GA was close to ideal, which exhibited trivial axial

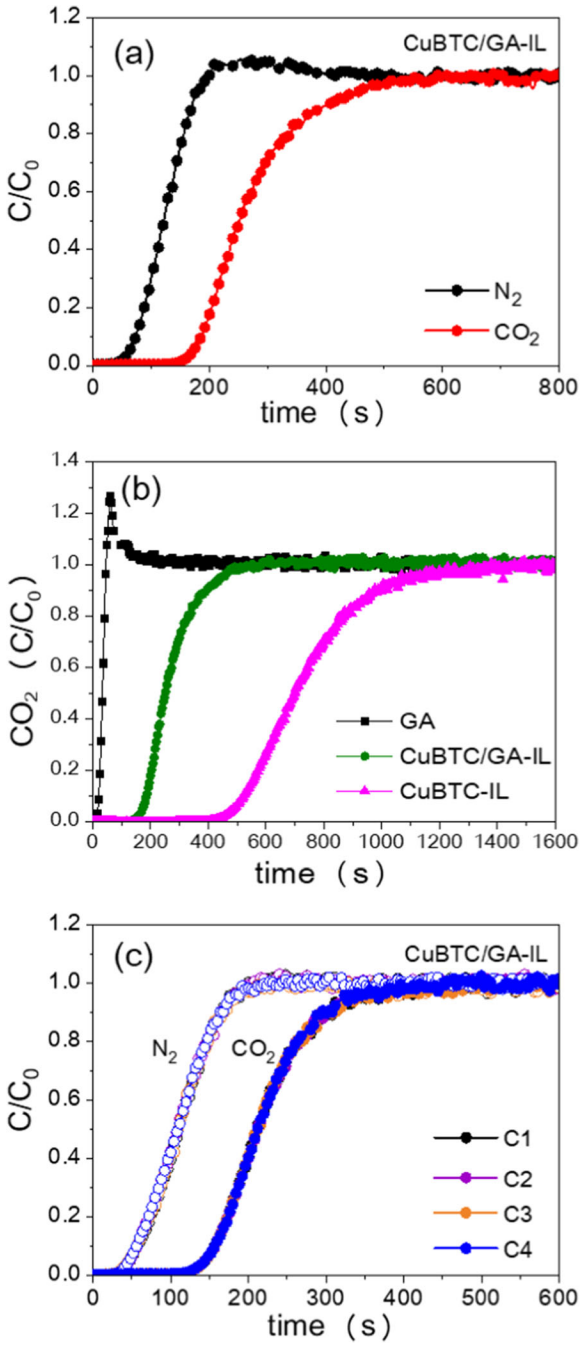

Fig. 4 **a** Breakthrough curves of CuBTC/GA-IL using a CO_2/N_2 gas mixture (20/80% *v*/*v*) at 298 K. **b** The CO_2 breakthrough curves of GA, CuBTC-IL, and CuBTC/GA-IL. **c** Recyclability of CuBTC/GA-IL for CO_2 adsorption/desorption at 298 K, using a gas mixture of CO_2/N_2 gas mixture (20/80% *v*/*v*)

dispersion and low mass transfer resistance due to the presence of macropores in GA. In addition, comparing the CO_2 breakthrough curves of GA, CuBTC/GA-IL, and CuBTC-IL, the front curve of GA was much steeper than that of CuBTC/GA-IL, and the front curve of CuBTC/GA-IL was much steeper than that of CuBTC, indicating that mass transfer was enhanced in CuBTC/GA-IL. These results demonstrated that the mass transfer resistance in the CuBTC/GA-IL is reduced due to the high effective diffusion of CO_2 in the meso-/macroporous GA, and the breakthrough time is longer compared with GA because of the integrated CuBTC. Moreover, CuBTC/GA-IL also exhibited good recycle stability (Fig. 4c), in which the breakthrough curves of CO_2 and N_2 were not changed after four adsorption/desorption cycles. In summary, the incorporation of microporous CuBTC into meso-/macroporous GA accompanied with IL additives gives rise to hierarchical CuBTC/GA-IL, which exhibited relatively high CO_2 uptake and low mass transfer resistance as well as good cyclability.

Conclusions

In this study, we reported an approach to synthesize structured CuBTC/GA-IL composite with preferential hierarchical pores at room temperature for carbon capture. It was demonstrated that incorporation of CuBTC into GA using IL additives endowed the composites with hierarchical pores that is favorable for mass transfer without significantly compensating the CO_2 adsorption capacity compared with CuBTC. Moreover, breakthrough experiments verified that CuBTC/GA-IL exhibited the lower mass transfer resistance and cycle stability, both of which benefit CO_2 capture. It should be noted that the reported strategy to incorporate microporous CuBTC into monolithic meso-/macroporous GA under the assistance of IL additives at room temperature in this study may be extended to other types of MOFs, ILs, and macroporous support matrix, which invites further investigations in the future. It should be also noted that except adsorption capacity and cyclability, the material cost should be also taken into account for practical application of CuBTC/GA-IL. The current lab cost of CuBTC/GA-IL is approximately $ 2.90 per gram, which may be remarkably reduced with the development of large-scale production techniques in the future.

Acknowledgments We thank the Analytical & Testing Center of Huazhong University of Science and Technology for the support.

Funding information This work was funded by the National Natural Science Foundation of China (NSFC) under Project Nos. 51836003 and 51606081.Data availabilityAll data generated or analyzed during this study are included in this published article and its supplementary information file.

Compliance with ethical standards

Conflict of interest The authors declare that they have no conflict of interest.

Abbreviations *rGO,* reduced graphene oxide; *GA,* graphene aerogel; *ZIF,* zeolitic imidazolate framework; *Zr,* zirconium; *MIL,* Matériaux de l'Institut Lavoisier; *BTC,* benzene-1,3,5-tricarboxylate; *MOFs,* metal-organic frameworks; *DMF,* N, N-dimethylformamide; *SEM,* scanning electron microscopy; *PXRD,* powder X-ray diffractometer

References

Anbia M, Hoseini V (2012) Development of MWCNT@MIL-101 hybrid composite with enhanced adsorption capacity for carbon dioxide. Chem Eng J 191:326–330

Bian Z, Zhu X, Jin T, Gao J, Hu J, Liu H (2014) Ionic liquid-assisted growth of $Cu_3(BTC)_2$ nanocrystals on graphene oxide sheets: towards both high capacity and high rate for CO_2 adsorption. Microporous Mesoporous Mater 200:159–164

Boothandford ME et al (2014) Carbon capture and storage update. Energy Environ Sci 7:130–189

Chen C, Feng N, Guo Q, Li Z, Li X, Ding J, Wang L, Wan H, Guan G (2018) Template-directed fabrication of MIL-101(Cr)/mesoporous silica composite: layer-packed structure and enhanced performance for CO_2 capture. J Colloid Interface Sci 513:891–902

Chui SS-Y, Lo SM-F, Charmant JPH, Orpen AG, Williams ID (1999) A chemically functionalizable nanoporous material $[Cu_3(TMA)_2(H_2O)_3]$n. Science 283:1140–1150

Furtado AMB, Liu J, Wang Y, LeVan MD (2011) Mesoporous silica–metal organic composite: synthesis, characterization, and ammonia adsorption. J Mater Chem 21:6698–6706

Garcia S, Gil M, Martín C, Pis J, Rubiera F, Pevida C (2011) Breakthrough adsorption study of a commercial activated carbon for pre-combustion CO_2 capture. Chem Eng J 171: 549–556

Ge L, Wang L, Rudolph V, Zhu Z (2013) Hierarchically structured metal–organic framework/vertically-aligned carbon nanotubes hybrids for CO_2 capture. RSC Adv 3:25360–25366

Gibbins, Chalmers J, Hannah (2008) Carbon capture and storage. Energy Policy 36:4317–4322

Gorka J, Fulvio PF, Pikus S, Jaroniec M (2010) Mesoporous metal organic framework-boehmite and silica composites. Chem Commun (Camb) 46:6798–6800

Inonu Z, Keskin S, Erkey C (2018) An emerging family of hybrid nanomaterials: metal–organic framework/aerogel composites. ACS Appl Nano Mater 1:5959–5980

Jiang M, Li H, Zhou L, Xing R, Zhang J (2018) Hierarchically porous graphene/ZIF-8 hybrid aerogel: preparation, CO_2 uptake capacity, and mechanical property. ACS Appl Mater Interfaces 10:827–834

Li J et al (2011) Carbon dioxide capture-related gas adsorption and separation in metal-organic frameworks. Coord Chem Rev 255:1791–1823

Li G, Pang S, Wu Y, Ouyang J (2018a) Enhanced removal of hydroquinone by graphene aerogel-Zr-MOF with immobilized laccase. Chem Eng Commun 205:698–705

Li H, Wang K, Sun Y, Lollar CT, Li J, Zhou H-C (2018b) Recent advances in gas storage and separation using metal–organic frameworks. Mater Today 21:108–121

Liu H-S, Lan Y-Q, Li S-L (2010) Metal−organic frameworks with diverse structures constructed by using capsule-like ligand and NiII based on ionothermal and hydrothermal methods. Cryst Growth Des 10:5221–5226

Liu Y, Ghimire P, Jaroniec M (2019) Copper benzene-1,3,5-tricarboxylate (Cu-BTC) metal-organic framework (MOF) and porous carbon composites as efficient carbon dioxide adsorbents. J Colloid Interface Sci 535:122–132

Mao J, Ge M, Huang J, Lai Y, Lin C, Zhang K, Meng K, Tang Y (2017) Constructing multifunctional MOF@rGO hydro-/aerogels by the self-assembly process for customized water remediation. J Mater Chem 5:11873–11881

Myers AL, Prausnitz JM (1965) Thermodynamics of mixed-gas adsorption. AICHE J 11:121–127

Na L, Zhang L, Zhang W, Hua R (2015) Room temperature synthesis and characterization of metal-organic framework $Cu_3(BTC)_2$. Gongneng Cailiao/J Funct Mater 46:12079–12081

Qiu L et al (2008) Hierarchically micro-and mesoporous metal-organic frameworks with tunable porosity. Angew Chem 47: 9487–9491

Rezaei F, Webley PA (2010) Structured adsorbents in gas separation processes. Sep Purif Technol 70:243–256

Rezaei F, Mosca A, Webley P, Hedlund J, Xiao P (2010) Comparison of traditional and structured adsorbents for CO_2 separation by vacuum-swing adsorption. Ind Eng Chem Res 49:4832–4841

Riaz MA, Hadi P, Abidi IH, Tyagi A, Ou X, Luo Z (2017) Recyclable 3D graphene aerogel with bimodal pore structure for ultrafast and selective oil sorption from water. RSC Adv 7:29722–29731

Shang W, Kang X, Ning H, Zhang J (2013) Shape and size controlled synthesis of MOF nanocrystals with the assistance of ionic liquid mircoemulsions. Langmuir 29:13168–13174

Trickett CA, Helal A, Al-Maythalony BA, Yamani ZH, Cordova KE, Yaghi OM (2017) The chemistry of metal–organic frameworks for CO_2 capture, regeneration and conversion. Nat Rev Mater 2:1–16

Wang X-S, Ma S, Sun D, Parkin S, Zhou H-C (2006) A mesoporous metal−organic framework with permanent porosity. J Am Chem Soc 128:16474–16475

Wang B, Xie L-H, Wang X, Liu X-M, Li J, Li J-R (2018) Applications of metal–organic frameworks for green energy and environment: new advances in adsorptive gas separation, storage and removal. Green Energy Environ 3:191–228

Xiang Z, Peng X, Cheng X, Li X, Cao D (2011) CNT@$Cu_3(BTC)_2$ and metal–organic frameworks for

separation of CO_2/CH_4 mixture. J Phys Chem C 115:19864–19871

Xiang S, He Y, Zhang Z, Wu H, Zhou W, Krishna R, Chen B (2012) Microporous metal-organic framework with potential for carbon dioxide capture at ambient conditions. Nat Commun 3:1–9

Ye R, Ni M, Xu Y, Chen H, Li S (2018) Synthesis of Zn-based metal–organic frameworks in ionic liquid microemulsions at room temperature. RSC Adv 8:26237–26242

Yu J, Xie LH, Li JR, Ma Y, Seminario JM, Balbuena PB (2017) CO_2 capture and separations using MOFs: computational and experimental studies. Chem Rev 117:9674–9754

Zhang X, Liang Q, Han Q, Wan W, Ding M (2016) Metal-organic frameworks@graphene hybrid aerogels for solid-phase extraction of non-steroidal anti-inflammatory drugs and selective enrichment of proteins. Analyst 141:4219–4226

Zhao Y, Zhang J, Han B, Song J, Li J, Wang Q (2011) Metal–organic framework nanospheres with well-ordered mesopores synthesized in an ionic liquid/CO_2/surfactant system. Angew Chem Int Ed 50:636–639

Publisher's note Springer Nature remains neutral with regard to jurisdictional claims in published maps and institutional affiliations.